(Received 1 August 2025, Accepted 4 September 2025, Scheduled 10 September 2025)

Broadband Efficient Reflective Linear Polarization Converter

Bianmei Zhang[1] and Xiaoming Liu[2,*]

[1] School of Medical Information, Wannan Medical College, Wuhu 241002, Anhui, China
[2] School of Physics and Electronic Information, Anhui Normal University, Wuhu 241002, Anhui, China

ABSTRACT: A broadband efficient reflective linear polarization converter has been developed using a metasurface. The converter consists of a U-shaped array integrated with cross dipoles. The U-shaped unit facilitates cross-polarization conversion, while the cross dipole serves to broaden the operational bandwidth. It has been demonstrated that the proposed converter can transform an incident linearly polarized wave into its orthogonally polarized reflected wave across a broadband frequency range of 18.94–51.03 GHz with a conversion efficiency exceeding 90%. The efficiency remains above 90% even as the incident angle increases to 45°, within the frequency ranges of 19.18–20.19 GHz, 26.01–30.93 GHz, and 48.8–49.77 GHz. The strong electric and magnetic responses at multi-resonances reveal the broadband polarization conversion mechanism. A prototype was fabricated to verify the performance. Measured results exhibit good consistency with the simulated ones.

1. INTRODUCTION

Metamaterials are artificially designed materials that exhibit many fascinating characteristics not found in naturally occurring materials [1–3]. They have given rise to several significant applications that involve the manipulation of electromagnetic (EM) waves, including wave absorption [4], negative refraction [5], and invisibility cloaks [6]. In particular, metasurfaces, which are two-dimensional manifestations of metamaterials, can provide unprecedented opportunities for the manipulation of electromagnetic (EM) waves in terms of amplitude, phase, and polarization at a sub-wavelength scale [7, 8]. It is highly desirable to control the polarization state of EM waves because many applications, such as remote sensing, radar detection, and wireless communication, are inherently sensitive to polarization. Conventional polarization devices are typically designed using birefringence or the Faraday effect, which often necessitate specific thicknesses and bulky configurations [9, 10]. Consequently, incorporating them into ultrathin devices, such as advanced sensors and nanophotonic devices, poses significant challenges.

Recently, metasurfaces have been utilized to facilitate the design of compact structures, particularly for polarization control, due to their advantages of low cost, thin profile, and easy fabrication [11–14]. Generally, polarization manipulation devices based on anisotropic metasurfaces can be classified into two categories: transmissive and reflective. A transmissive polarization converter using a single substrate has been developed in [15], but this design tends to be a narrowband operation. To attain broadband operation, multilayer structures are employed in [16, 17]. However, the complex structure is less favored for fabrication. In comparison to transmissive polarization converters, many reflective polarization converters can provide superior performance using a simpler structure, due to the presence of metal plates [18–20].

For instance, a reflective polarization converter that employs multiple resonances and a high impedance surface was proposed to achieve cross-polarization conversion [21]. Using meander lines and cut wire, Zheng et al. [22] reported a broadband linear-cross polarization converter, with a conversion efficiency over 88%. Similarly, highly efficient polarization conversion was realized using a cross-shaped resonator [23]. The bandwidth can be expanded by stacking multiple structural layers [24], but the design works for normal incidence. The design proposed in [25] provides a 67% bandwidth and 30° angular stability. Another design can improve the bandwidth to 87.1% [26], yet it exhibits significant sensitivity to the angle of incidence, with angular stability below 20°. Further effort was made using nested circular ring-shaped metasurface [27]. The angular stability reaches up to 45°, but the conversion efficiency remains only above 80%. Furthermore, high angular stability polarization conversion is presented based on the bending of metallic lines [28]. However, the design only has an 18% bandwidth at an incident angle of 60°. It is evident that there is significant potential for achieving broadband cross-polarization conversion with high efficiency and good angular stability.

In this study, we focus on the development of a broadband efficient reflective linear polarization converter. The converter consists of a U-shaped array integrated with cross dipoles. It will be shown that high-efficiency cross-polarization conversion can be achieved under x-polarized incidence within the broadband frequency range of 18.94 to 51.03 GHz. Owing to the structural symmetry, similar results can also be derived for y-polarized incidence. To clarify the mechanism of broadband polarization conversion, the surface currents distribution has been analyzed at four resonances of 19.9 GHz, 26.3 GHz, 37.7 GHz, and 49.1 GHz. Besides, the unit cell size is nearly

* Corresponding author: Xiaoming Liu (xiaoming.liu@ahnu.edu.cn).

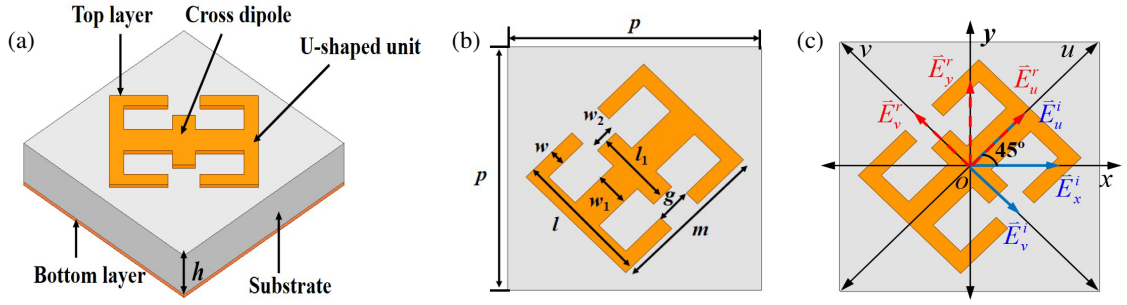

FIGURE 1. The schematic of unit cell. (a) Perspective view, (b) front view, (c) electric field decomposition.

$0.41\lambda_c$, where λ_c denotes the center frequency wavelength within the operational band. This miniaturized property results in good angular stability. The polarization conversion rate (PCR) is greater than 90% at angles as high as 45° within the frequency ranges of 19.18–20.19 GHz, 26.01–30.93 GHz, and 48.8–49.77 GHz. A prototype has been fabricated to verify the performance of this design.

2. THEORY ANALYSIS AND DESIGN

The structural design of the proposed polarization converter is presented in Fig. 1. The unit cell consists of two metallic layers separated by a dielectric substrate. The top layer features a pattern of the U-shaped unit integrated with a cross dipole, while the bottom layer is a purely metallic plane. To achieve polarization conversion, the metallic pattern on the top layer is slantly arranged. The metallic layers are modeled as a copper film with a thickness of 0.018 mm. The used dielectric substrate is low-loss F4B, which has a dielectric constant of 2.65 and a loss tangent of 0.001. The simulation and analysis of the proposed converter were conducted through Ansys High Frequency Structure Simulator (HFSS) 2021 software. In the simulation, periodic boundary conditions for the unit structure were established within the *xoy* plane, and the Floquet port was configured along the z-direction. After optimization, the structural dimensions of the unit cell are as follows: $p = 3.5$ mm, $h = 1.2$ mm, $l = 1.95$ mm, $l_1 = 1.1$ mm, $w = 0.22$ mm, $w_1 = 0.47$ mm, $w_2 = 0.36$ mm, $g = 0.5$ mm, and $m = 2.3$ mm.

To analyze the working mechanism of the proposed converter, an x-polarized incident wave can be decomposed into two perpendicular components along the u- and v-axes shifted to the x-axis by $\pm 45°$, as depicted in Fig. 1(c). Hence, the incident and reflected waves can be expressed as [25]

$$\vec{E}^{\,i} = E_u^i \vec{u} - E_v^i \vec{v} \tag{1}$$

$$\vec{E}^{\,r} = E_u^r \vec{u} + E_v^r \vec{v} \tag{2}$$

where $\vec{u}$ and $\vec{v}$ represent unit vectors in the u- and v-directions, respectively. The superscripts i and r indicate the incident and reflected waves, respectively; the subscripts u and v denote the polarization direction of EM wave. Further, the reflected wave can also be written as [29]

$$\vec{E}^{\,r} = \left(r_{uu} E_u^i e^{j\varphi_{uu}} + r_{uv} E_v^i e^{j\varphi_{uv}}\right) \vec{u} + \left(r_{vv} E_v^i e^{j\varphi_{vv}} + r_{vu} E_u^i e^{j\varphi_{vu}}\right) \vec{v} \tag{3}$$

here r_{uu} and r_{vv}, r_{vu} and r_{uv} represent the co-polarized and cross-polarized reflection coefficients in the u- and v-directions, respectively; φ_{uu} and φ_{vv}, φ_{vu} and φ_{uv} represent the co-polarized and cross-polarized reflection phases in the u- and v-directions, respectively.

When $r_{uu} = r_{vv} \cong 1$, $r_{vu} = r_{uv} \cong 0$, and $\Delta\varphi_{uv} = \varphi_{uu} - \varphi_{vv} \approx \pm 180°$, the reflected wave will be aligned in the y-direction. Similarly, the reflection coefficients can be defined as [30]

$$\begin{cases} r_{xx} = E_x^r / E_x^i \\ r_{yx} = E_y^r / E_x^i \end{cases} \tag{4}$$

where x and y signify the polarization direction of EM wave; r_{xx} and r_{yx} denote the co-polarized and cross-polarized reflection coefficients, respectively.

To verify the polarization conversion, the reflection coefficients r_{uu} and r_{vv} were analyzed under u- and v-polarized incident waves. As depicted in Fig. 2, the amplitudes of r_{uu} and r_{vv} are nearly equal to 1, and those of r_{vu} and r_{uv} are nearly 0 in the frequency range of 19.06–51.09 GHz. Moreover, the phase retardation ranges from 160° to 200° or from −160° to −200° within this operational band. Such a result demonstrates that the proposed converter possesses good polarization conversion capabilities over a broad frequency bandwidth.

For x-polarized normal incidence, the simulated reflection coefficients r_{xx} and r_{yx} are shown in Fig. 3(a). It can be observed that the value of r_{xx} is less than −10 dB, while r_{yx} is larger than −0.63 dB in the frequency range of 19.06–51.09 GHz. The result indicates that highly efficient cross-polarization conversion is generated under an x-polarized incident wave. Fig. 3(b) shows the PCR across the entire frequency band, which is calculated using [31]

$$\mathrm{PCR} = r_{yx}^2 / \left(r_{yx}^2 + r_{xx}^2\right) = 1 - r_{xx}^2 / \left(r_{yx}^2 + r_{xx}^2\right) \tag{5}$$

It can be observed that the PCR value is greater than 90% within the frequency range of 19.06–51.09 GHz, approaching a value of unity at four specific resonance frequencies: 19.9 GHz, 26.3 GHz, 37.7 GHz, and 49.1 GHz. Apparently, most of the energy from the x-polarized incident wave is converted into the y-polarized reflected wave across this broad frequency range. It is worth mentioning that when a right circularly polarized wave illuminates the proposed converter, it can also convert the

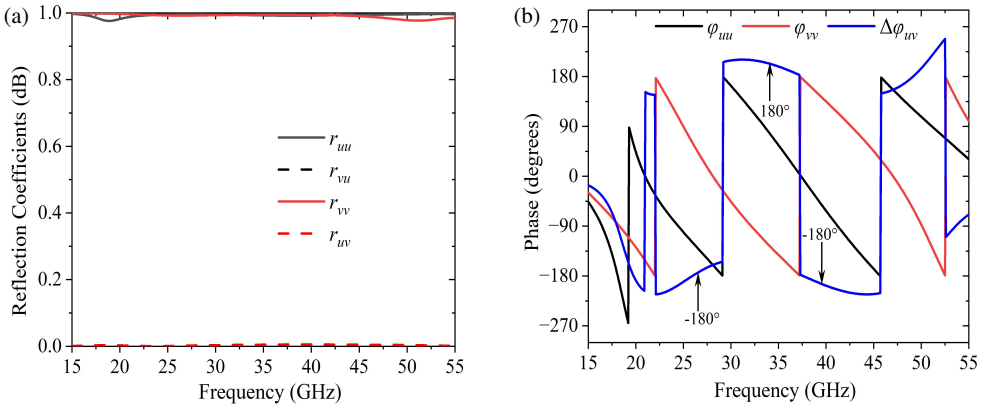

FIGURE 2. Reflection coefficients under u- and v-polarized normal incidence. (a) Amplitude, (b) phase.

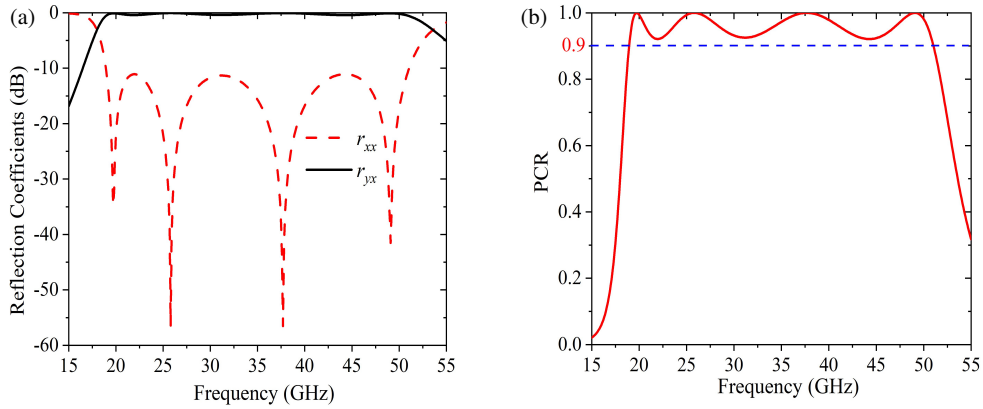

FIGURE 3. Simulated reflection results under x-polarized normal incidence. (a) Amplitude, (b) PCR.

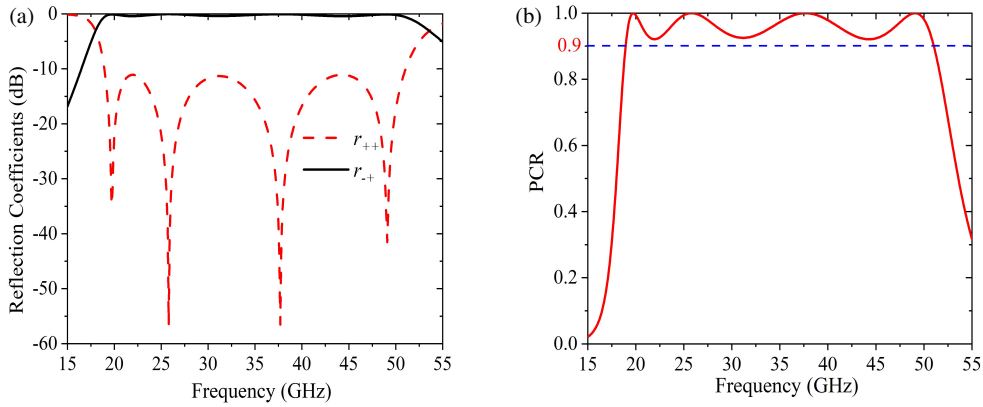

FIGURE 4. Simulated reflection results under right circularly polarized incidence. (a) Reflection coefficients (the subindices "+" and "−" denote right circularly polarized and left circularly polarized waves, respectively), (b) PCR.

incident circularly polarized wave into its cross-polarized wave across the same frequency band (see Fig. 4).

In addition, Fig. 5(a) shows the reflection results of r_{xx} and r_{yx} under different incident angles. Apparently, the incident angles have a significant impact on the operational bandwidth and conversion efficiency of the proposed converter. It can be observed that as the incident angle increases, the cross-polarization reflection coefficient r_{yx} experiences a reduction, and the co-polarization reflection coefficient r_{xx} undergoes drastic fluctuations at higher frequencies. Indeed, when EM waves encounter a dielectric plate at an oblique angle of incidence, they will create a propagation phase that surpasses one under conditions of normal incidence [17, 25], resulting in destructive interference at the metasurface's surface. With an increase of incident angle, the destructive interference becomes pronounced at higher frequencies. Therefore, it is always chal-

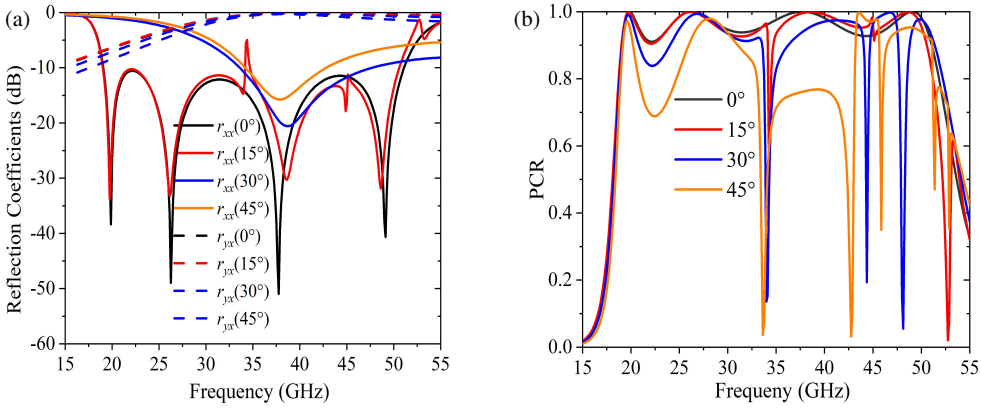

FIGURE 5. Simulated reflection results at various oblique incidence. (a) Amplitude, (b) PCR.

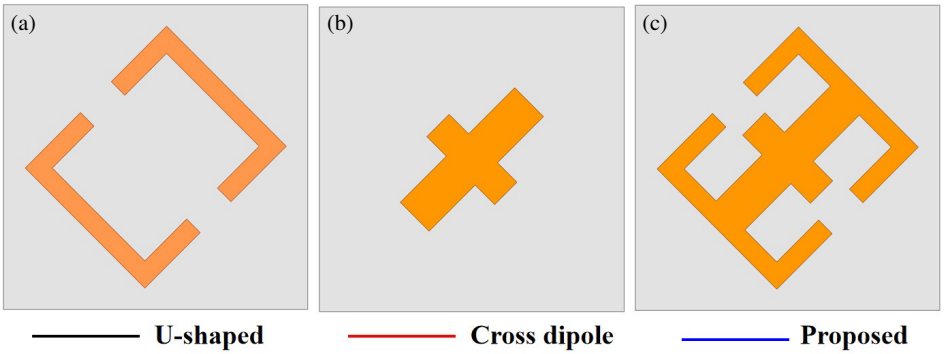

FIGURE 6. Structural evolution. (a) U-shaped unit, (b) cross dipole, and (c) proposed structure.

lenging to work with large angles and a broad bandwidth. One reason is that multi-resonances are required for broadband polarization conversion to ensure effective bandwidth. However, higher-order resonances cannot be always guaranteed at large angles of incidence.

A popular method involves minimizing the unit cell through a folded pattern. The technique is used to extend the current path in this design. The unit size is 0.41 wavelength at the center frequency 34.99 GHz. The miniaturized structure reduces the distribution of the electric field caused by variations in the incident angle. Additionally, a low-loss F4B dielectric material with a thickness of 1.2 mm is employed to ensure stable polarization conversion performance at large angles. Fig. 5(b) shows the simulated results of PCR for different incident angles. Although the operational bandwidth of PCR exceeding 90% rapidly declines as the incident angle increases from 0° to 45°, the PCR still sustains a level of 90% within the frequency ranges of 19.18–20.19 GHz, 26.01–30.93 GHz, and 48.8–49.77 GHz, even when the incident angle reaches 45°.

3. DESIGN EVOLUTION

The design of a broadband efficient polarization converter requires the tuning of the unit cell's multiple resonances. Considering that the structure is composed of U-shaped units integrated with a cross dipole, the structural evolution is investigated in Fig. 6. The design process involves three key stages: initially, a U-shaped structure is engineered to break the polarization symmetry of the incident electric field and to excite the resonant current within the unit, causing the polarization direction of the incident wave to change from x-polarization to y-polarization. As shown in Fig. 7, two resonances for the U-shaped structure are stimulated at 31.6 GHz and 50.5 GHz. The reflection amplitude of r_{xx} is below -8.58 dB, while that of r_{yx} is above -0.71 dB over the frequency range of 26.94–52.9 GHz, achieving the cross-polarization conversion with a PCR exceeding 85% and near-unity value at two resonances.

Next, a cross dipole is utilized to control the resonant properties at higher frequency, thus creating a resonance at 54.6 GHz. In fact, cross dipole is commonly used in traditional antenna design to address issues such as narrow bandwidth, low gain, and high profile [23]. In this design, the technique is employed to expand the bandwidth of polarization conversion. After the synergistic integration of two structures, a lower frequency resonance is generated at 19.9 GHz. Notably, the U-shaped structure can enhance the amplitude condition of cross-polarization conversion in the lower band, but it contributes less in the higher band. This tendency is exactly the opposite for cross dipoles. It is observed that the reflection amplitudes of r_{xx} and r_{yx} are continuous at four closely related resonances: 19.9 GHz, 26.3 GHz, 37.7 GHz, and 49.1 GHz, ensuring broadband operation with a PCR greater than 90% over the frequency range of 19.06–51.09 GHz.

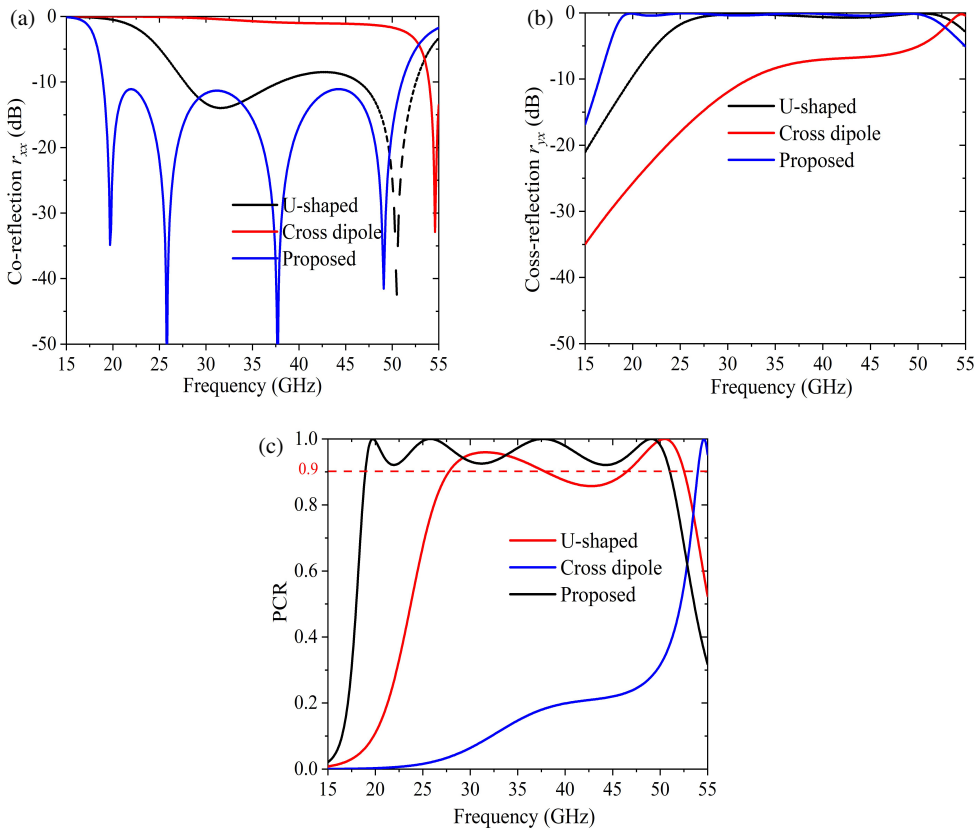

FIGURE 7. The reflection results of structural evolution. (a) Co-reflection, (b) cross-reflection, (c) PCR.

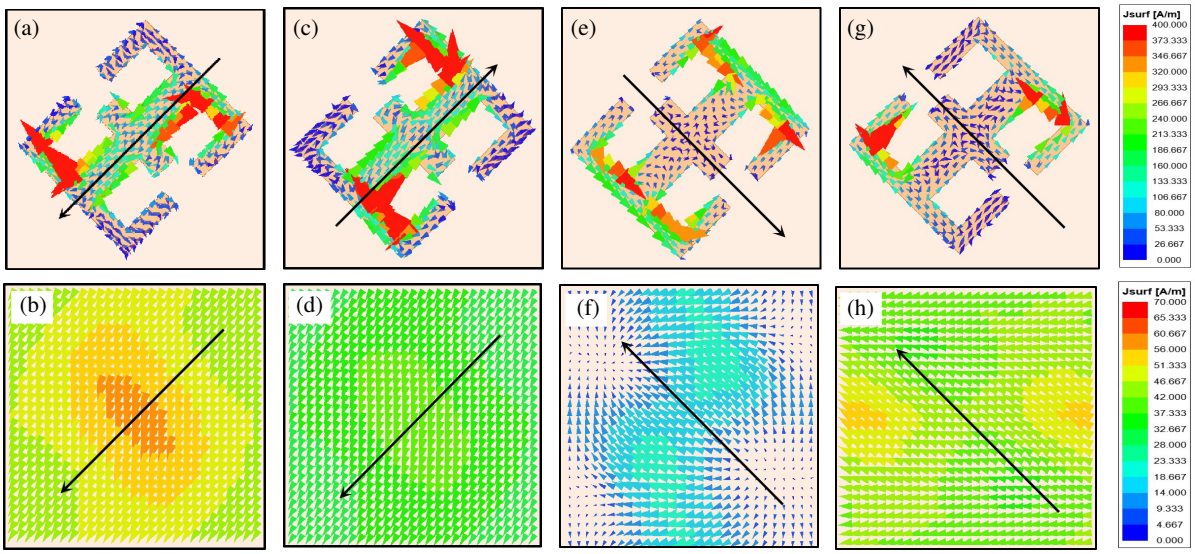

FIGURE 8. Surface current distributions of the top and bottom layers at four resonant frequencies. (a), (b) 19.9 GHz, (c), (d) 26.3 GHz, (e), (f) 37.7 GHz, and (g), (h) 49.1 GHz.

4. SURFACE CURRENT DISTRIBUTIONS

To understand the mechanism of polarization conversion from the proposed converter, the surface current distributions of the top and bottom layers are analyzed at four different resonant frequencies: 19.9 GHz, 26.3 GHz, 37.7 GHz, and 49.1 GHz, as shown in Fig. 8. At 19.9 GHz, the surface current on the top layer is mainly concentrated on the surface of the cross dipole, traversing from the top-right to the bottom-left. The orientation of the current is parallel to that on the bottom layer. A similar phenomenon can be observed at 49.1 GHz, where the U-shaped unit primarily contributes to the current distribution. This indicates that the resonances at 19.9 GHz and 49.1 GHz

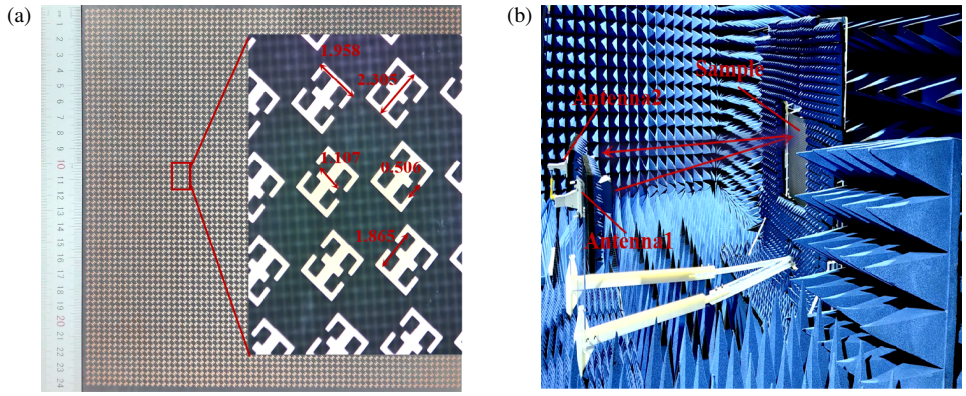

FIGURE 9. (a) Measurement sample, (b) experimental setup.

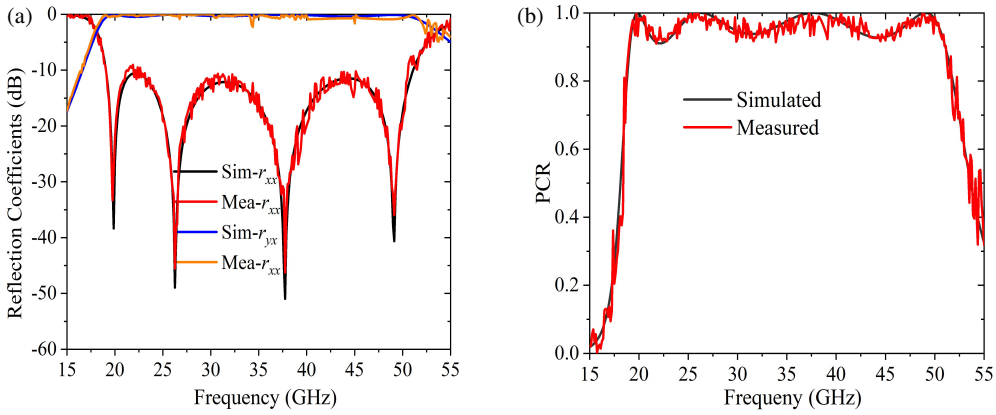

FIGURE 10. Comparison between measured and simulated results. (a) Reflection coefficients, (b) PCR.

mainly exhibit the electrical properties that enhance the electric field within the dielectric substrate. However, the current distributions on the top and bottom layers are antiparallel at 26.3 and 37.7 GHz, resulting in a magnetic field within the dielectric substrate. The design can be considered an artificial magnetic conductor because it exhibits a strong magnetic flux, with a magnetic permeability value that exceeds that of free space. In other words, the property of multiple resonances, induced by strong electric and magnetic responses, reveals a broadband conversion mechanism of linear polarization between the top and bottom layers.

5. FABRICATION AND MEASUREMENT

To validate this design, a prototype was fabricated which contains 32 × 32 unit cells. As shown in Fig. 9(a), the sample was etched onto an F4B substrate with dimensions of 112 × 112 mm^2. The fabrication accuracy was examined using an industrial microscope, within a tolerance of 10 µm.

The measurement setup was depicted in Fig. 9(b). The horn antenna was connected to a Ceyear AV3672D performance network analyzer (VNA) calibrated using the standard through-reflect-line (TRL) calibration method. The centers of horn antennas and fabricated sample were placed at the same height and surrounded by radio frequency (RF) absorbing materials. To ensure greater accuracy, a time-gating technique was utilized to eliminate residual noise. A metallic ground plane of the same size as the sample was employed to obtain the path loss for the reflection coefficient. During measurement, two antennas were preserved with consistent polarization orientations for co-polarized reflection. Conversely, for cross-polarized reflection, the polarization orientations were adjusted to be mutually orthogonal, so that the PCR can be obtained.

The measured results for reflection coefficients and PCR are shown in Fig. 10. The measurement and simulation results are in good agreement. There are four resonant frequencies within the frequency range of 15–51.13 GHz. The reflection coefficient r_{xx} is below -10 dB, while the reflection coefficient r_{yx} is above -1 dB in this frequency range. Further, it is observed that the measured PCR is higher than 90%. The results demonstrate the highly efficient polarization conversion from x-polarized to y-polarized waves across a broad frequency range. Due to the structural symmetry, similar results can also be derived for y-polarized incident waves. However, compared to the simulated results, there are some discrepancies in the measured ones. This may be due to errors related to fabrication and measurement processes, including background noise and misalignment of the horn antennas.

Finally, a comparison of proposed converter with the reflective polarization converters previously reported in the literature is carried out in Table 1. It is evident that the proposed con-

TABLE 1. Comparison of the reflective polarization converters.

Ref.	Operating Bandwidth (GHz)	Relative Bandwidth	PCR	Size
[1]	8.75–17.75	67.92%	90%	$370 \times 370 \times 2\,\text{mm}^3$ $(16.34 \times 16.34 \times 0.09\lambda_c^3)$
[7]	6.36–6.59 10.54–13.56	3.55% 25.06%	90%	$304 \times 304 \times 2.4\,\text{mm}^3$ $(6.56 \times 6.56 \times 0.05\lambda_c^3)$
[17]	12.4–27.96	77.11%	90%	$250 \times 250 \times 1.6\,\text{mm}^3$ $(16.82 \times 16.82 \times 0.11\lambda_c^3)$
[20]	7.74–14.44	60.41%	90%	$270 \times 270 \times 3\,\text{mm}^3$ $(9.98 \times 9.98 \times 0.11\lambda_c^3)$
[22]	6.53–12.07	59.57%	88%	$243 \times 243 \times 3.1\,\text{mm}^3$ $(7.53 \times 7.53 \times 0.10\lambda_c^3)$
[25]	10.2–20.5	67.1%	90%	$300 \times 300 \times 2\,\text{mm}^3$ $(15.35 \times 15.35 \times 0.10\lambda_c^3)$
[30]	17.4–18.9	8.26%	90%	$450 \times 450 \times 1.5\,\text{mm}^3$ $(27.23 \times 27.23 \times 0.09\lambda_c^3)$
[32]	5–10.8	73%	80%	$305 \times 305 \times 2.4\,\text{mm}^3$ $(8.03 \times 8.03 \times 0.06\lambda_c^3)$
This work	18.94–51.03	91.73%	90%	$112 \times 112 \times 1.2\,\text{mm}^3$ $(13.06 \times 13.06 \times 0.14\lambda_c^3)$

verter can provide a thinner thickness of 1.2 mm and broadband operation ranging from 18.94 to 51.03 GHz with PCR greater than 90%, making it suitable for a variety of wideband applications, including 5G millimeter waves, multi-frequency radars, and "thin and light" requirements of small communication terminals and satellite modules.

6. CONCLUSION

A broadband efficient reflective polarization converter has been presented using U-shaped unit and cross dipole. It has shown that the proposed converter can convert a linearly polarized incident wave into its cross-polarized reflected wave in the frequency range of 18.94–51.03 GHz. The PCR is greater than 90% in this broadband range and approaches 100% at 19.9 GHz, 26.3 GHz, 37.7 GHz, and 49.1 GHz. Besides, the miniaturized structure results in good angular stability, with the PCR exceeding 90% at angles as high as 45° within the frequency ranges of 19.18–20.19 GHz, 26.01–30.93 GHz, and 48.8–49.77 GHz. The surface current distribution from multiple resonances has been analyzed to reveal the mechanism of linear-to-cross polarization conversion. The proposed converter provides a promising solution for applications in remote sensing, radar detection, and wireless communication systems.

ACKNOWLEDGEMENT

The authors thank the supports from the National Natural Science Foundation of China (No. 61871003), the Natural Science Foundation of Anhui Province (No. 2308085Y02), and the Doctoral Research Sart-Up Funds of Wannan Medical College (No. X600100173).

REFERENCES

[1] Nochian, P. and Z. Atlasbaf, "An ultra-wideband thin metamaterial linear cross-polarization conversion," *Scientific Reports*, Vol. 15, No. 1, 3062, 2025.

[2] You, J., Q. Ma, L. Zhang, C. Liu, J. Zhang, S. Liu, and T. Cui, "Electromagnetic metamaterials: From classical to quantum," *Electromagnetic Science*, Vol. 1, No. 1, 1–33, 2023.

[3] Yang, H., Y. He, M. S. Tong, L. T. Guo, P. Li, and Y. J. Zhang, "A reflection-transmission multifunctional polarization conversion metasurface," *IEEE Transactions on Antennas and Propagation*, Vol. 72, No. 6, 5099–5109, 2024.

[4] Tuan, T. S. and N. T. Q. Hoa, "Numerical study of an efficient broadband metamaterial absorber in visible light region," *IEEE Photonics Journal*, Vol. 11, No. 3, 1–10, 2019.

[5] Chen, C.-Y., M.-C. Hsu, C. D. Hu, and Y. C. Lin, "Natural negative-refractive-index materials," *Physical Review Letters*, Vol. 127, No. 23, 237401, 2021.

[6] Lin, J.-H., T.-J. Yen, and T.-Y. Huang, "Design of annulus-based dielectric metamaterial cloak with properties of illusion optics," *Journal of Optics*, Vol. 22, No. 8, 085101, 2020.

[7] Wahidi, M. S., M. I. Khan, F. A. Tahir, and H. Rmili, "Multifunctional single layer metasurface based on hexagonal split ring resonator," *IEEE Access*, Vol. 8, 28 054–28 063, 2020.

[8] Guo, Q., F. Hao, M. Qu, J. Su, and Z. Li, "Multiband multifunctional polarization converter based on reconfigurable metasurface," *IEEE Antennas and Wireless Propagation Letters*, Vol. 23, No. 4, 1241–1245, 2024.

[9] Zhang, T., H. Wang, C. Peng, Z. Chen, G.-M. Yang, and X. Wang, "Multifunctional polarization converters based on linear-to-circular polarization decomposition reflective surfaces," *IEEE Transactions on Antennas and Propagation*, Vol. 72, No. 11, 8476–8487, 2024.

[10] Yang, H., S. C. Wang, P. Li, Y. He, and Y. J. Zhang, "A broadband multifunctional reconfigurable polarization conver-

sion metasurface," *IEEE Transactions on Antennas and Propagation*, Vol. 71, No. 7, 5759–5767, 2023.

[11] Ahmad, I., W. Ali, R. Zhou, S. B. Jamali, and L. Deng, "Reflective linear polarization converter with multimode, dual band and high efficiency," *Physica Scripta*, Vol. 100, No. 2, 025502, 2025.

[12] Liu, C., F. Yang, S. Xu, and M. Li, "Reconfigurable metasurface: A systematic categorization and recent advances," *Electromagnetic Science*, Vol. 1, No. 4, 1–23, 2023.

[13] Huang, S., Z. Wang, L. Qiu, P. Zhang, Y. Liu, S. Fang, and L. Deng, "Wideband and function-switchable polarization converter based on multi-mode active metasurface," *AEU — International Journal of Electronics and Communications*, Vol. 162, 154578, 2023.

[14] Kundu, D., J. Singh, D. Singh, and A. Chakrabarty, "Design and analysis of broadband ultrathin reflective linear-to-circular polarization converter using polygon-based anisotropic-impedance surface," *IEEE Transactions on Antennas and Propagation*, Vol. 69, No. 8, 5154–5159, 2021.

[15] Gao, X., X. Han, W.-P. Cao, H. O. Li, H. F. Ma, and T. J. Cui, "Ultrawideband and high-efficiency linear polarization converter based on double V-shaped metasurface," *IEEE Transactions on Antennas and Propagation*, Vol. 63, No. 8, 3522–3530, 2015.

[16] Liu, K., G. Wang, T. Cai, and T. Li, "Dual-band transmissive circular polarization generator with high angular stability," *Optics Express*, Vol. 28, No. 10, 14 995–15 005, 2020.

[17] Zhao, J., Y.-J. Cheng, T.-J. Huang, and P.-K. Liu, "A dual-band linear-to-circular polarization converter with robustness under oblique incidences," *Microwave and Optical Technology Letters*, Vol. 63, No. 1, 361–366, 2021.

[18] Omar, A. A., W. Hong, A. Al-Awamry, and A.-E. Mahmoud, "A single-layer vialess wideband reflective polarization rotator utilizing perforated holes," *IEEE Antennas and Wireless Propagation Letters*, Vol. 19, No. 12, 2053–2056, 2020.

[19] Zafar, J., H. Z. Khan, A. Jabbar, J. U. R. Kazim, M. U. Rehman, A. M. Siddiqui, Q. H. Abbasi, and M. A. Imran, "Multi-band reflective metasurface for efficient linear and circular polarization conversion," *Optical and Quantum Electronics*, Vol. 57, No. 2, 149, 2025.

[20] Zheng, Q., C. Guo, G. A. E. Vandenbosch, P. Yuan, and J. Ding, "Dual-broadband highly efficient reflective multi-polarisation converter based on multi-order plasmon resonant metasurface," *IET Microwaves, Antennas & Propagation*, Vol. 14, No. 9, 967–972, 2020.

[21] Kaya, Y., U. C. Hasar, H. Ozturk, and G. Ozturk, "Multifunctional, multi-band, low-profile, ultra-thin, and cost-effective metasurface-based polarization converter," *Measurement*, Vol. 248, 116894, 2025.

[22] Zheng, Q., C. Guo, and J. Ding, "Wideband metasurface-based reflective polarization converter for linear-to-linear and linear-to-circular polarization conversion," *IEEE Antennas and Wireless Propagation Letters*, Vol. 17, No. 8, 1459–1463, 2018.

[23] Liu, Z., B. Zhao, C. Jiao, L. Zhao, and X. Han, "Broadband cross-polarization conversion metasurface based on cross-shaped resonators," *Applied Physics A*, Vol. 127, No. 11, 825, 2021.

[24] Zheng, Q., C. Guo, G. A. E. Vandenbosch, P. Yuan, and J. Ding, "Ultra-broadband and high-efficiency reflective polarization rotator based on fractal metasurface with multiple plasmon resonances," *Optics Communications*, Vol. 449, 73–78, 2019.

[25] Karamirad, M., C. Ghobadi, and J. Nourinia, "Metasurfaces for wideband and efficient polarization rotation," *IEEE Transactions on Antennas and Propagation*, Vol. 69, No. 3, 1799–1804, 2021.

[26] Pramanik, S., S. Bhaumik, S. Bhunia, and C. Koley, "Broadband metasurface-based reflective polarization converter," *Frequenz*, Vol. 79, No. 5-6, 241–246, 2025.

[27] Kaya, Y., "Ultra-thin reflective multifunctional polarization converter with nested circular ring-shaped metasurface-based for C- and X-band applications," *Optical and Quantum Electronics*, Vol. 55, No. 4, 335, 2023.

[28] Ye, H. and Y. Zhang, "Design of polarization convert metasurface element with high angle stability," *Optics Express*, Vol. 32, No. 10, 17 103–17 115, 2024.

[29] Pramanik, S., S. C. Bakshi, C. Koley, D. Mitra, A. Monti, and F. Bilotti, "Active metasurface-based reconfigurable polarization converter with multiple and simultaneous functionalities," *IEEE Antennas and Wireless Propagation Letters*, Vol. 22, No. 3, 522–526, 2023.

[30] Liu, X., J. Zhang, W. Li, R. Lu, L. Li, Z. Xu, and A. Zhang, "Three-band polarization converter based on reflective metasurface," *IEEE Antennas and Wireless Propagation Letters*, Vol. 16, No. 16, 924–927, 2017.

[31] Wang, P., Y. Zhang, Y. Wang, H.-C. Zhou, and Z.-M. Yan, "Multifunctional polarization converter based on multilayer reconfigurable metasurface," *Defence Technology*, Vol. 28, No. 10, 136–145, 2023.

[32] Khan, M. I., Q. Fraz, and F. A. Tahir, "Ultra-wideband cross polarization conversion metasurface insensitive to incidence angle," *Journal of Applied Physics*, Vol. 121, No. 4, 045103, 2017.